Title: Gating mechanism of cardiac ryanodine receptor 2 upon calcium ion binding

Authors: Takuya Kobayashi[1]†, Akihisa Tsutsumi[2]†, Nagomi Kurebayashi[1], Kei Saito[3], Masami Kodama[4], Takashi Sakurai[1], Masahide Kikkawa[2], Takashi Murayama[1]* and Haruo Ogawa[4]*.

Affiliations:

[1]Department of Cellular and Molecular Pharmacology, Juntendo University Graduate School of Medicine.

[2]Department of Cell Biology and Anatomy, Graduate School of Medicine, The University of Tokyo.

[3]Department of Life Sciences, Graduate School of Arts and Sciences, The University of Tokyo.

[4]Institute for Quantitative Biosciences, The University of Tokyo.

*Correspondence to: Email: takashim@juntendo.ac.jp (T.M.); haru@iqb.u-tokyo.ac.jp (H.O.)

†These authors contributed equally to this work.

Abstract: Cardiac ryanodine receptor (RyR2) is a large Ca^{2+} release channel in the sarcoplasmic reticulum and indispensable for excitation-contraction coupling in the heart. RyR2 is activated by Ca^{2+} and RyR2 mutations have been implicated in severe arrhythmogenic heart diseases. Yet, the structural basis underlying channel opening and how mutations affect the channel remain unknown. Here, we combined high-resolution structures determined by cryo-electron microscopy with quantitative functional analysis of channels carrying various mutations in specific residues. We demonstrated that interactions close to the channel pore are important for stabilizing the channel in the closed state and those in the surrounding regions are essential for channel opening. Our results reveal mechanisms underlying channel opening upon Ca^{2+} binding and alterations by pathogenic mutations of RyR2 at the atomic level.

One Sentence Summary: Key movements and interactions in RyR2 during cardiac Ca^{2+} channel opening are clarified at the atomic level.

Main Text: Cardiac muscle contraction is triggered by an influx of Ca^{2+} into the cytosol through L-type voltage-dependent Ca^{2+} channels in the plasma membrane. This increase in Ca^{2+} activates the cardiac ryanodine receptor (RyR2) in the sarcoplasmic reticulum to release large amount of Ca^{2+}, a process known as Ca^{2+}-induced Ca^{2+} release (CICR) (*1, 2*). RyR2 is a homotetramer and the largest ion channel identified to date. Its total molecular weight is ~2.2 Mda, with each monomer composed of ~5,000 amino acid residues and comprising a large N-terminal mushroom-like structure of the cytoplasmic domain and C-terminal transmembrane (TM) region (*3, 4*). Nearly 300 pathogenic mutations in RyR2 that alter channel activity by gain-of-function or loss-of-function mechanisms have been reported as arrhythmogenic heart diseases, including

catecholaminergic polymorphic ventricular tachycardia (CPVT) (*5-8*), left ventricular non compaction (LVNF) (*9-11*), and idiopathic ventricular fibrillation (IVF) (*12-14*).

The first reported structure of RyR2, derived from pig heart, was in the closed state in the presence of EGTA and in the open state with Ca^{2+} and PCB95 (*15*). This was followed by reports on RyR2 activity modulation by regulatory proteins, such as calmodulin (*16*) and FKBP12.6 (*17*). These reports along with prior studies on RyR1 (see (*18*) for a recent review) provided insights into RyR2 domain organizations, conformational changes upon channel opening, and the binding sites for ligands and regulatory proteins. Structural analysis has indicated the importance of intra/inter-domain interactions for long-range allosteric regulation of channel gating, yet the roles of individual interaction remains unknown. Thus, the fundamental mechanism underlying channel opening at the atomic level remains to be elucidated. Moreover, it remains unclear how pathogenic mutations alter the channel activity.

To identify key movements and interactions in the channel opening, we here obtained high-resolution structures of recombinant mouse RyR2 by cryo-electron microscopy (EM) single-particle analysis. Then, functional analysis was conducted with RyR2 channels carrying mutations in amino-acid residues in the proposed interactions to clarify their roles during channel gating. Moreover, structures of two mutant channels were determined to address molecular mechanism of alteration. We demonstrated that interactions in the regions close to the channel pore are important for stabilizing the channel in the closed state and those in the surrounding regions are essential for channel opening. Our results reveal mechanisms underlying channel opening upon Ca^{2+} binding and explain how pathogenic mutations alter channel activity at the atomic level.

Overall conformational changes in RyR2 associated with Ca^{2+} binding

Recombinant mouse RyR2, expressed and purified from HEK293 cells using FKBP12.6 affinity chromatography (fig. S1A) (*19*), formed homogeneous tetrameric channels (fig. S1B). To precisely trace the Ca^{2+}-induced RyR2 structural changes, a fully open state without any activating ligands other than Ca^{2+} is necessary. Thus, we adopted high salt conditions, which markedly enhance channel activity with Ca^{2+} alone (fig. S1, C–E) (*20, 21*). We performed cryo-EM single-particle analysis in the presence of 1 mM EGTA and 100 μM Ca^{2+} for closed and open states, respectively. Three-dimensional (3D) classification including focused classification analysis using the TM region revealed two and three classes in the presence of EGTA and Ca^{2+}, respectively (fig. S2; table S1). No major differences were observed between the closed and open states among the classes. Therefore, subsequent analysis was performed using the class with the highest resolution (before the final classification in the closed state and class 1 in the open state; table S1). The overall resolution of the final model was 3.3 Å and 3.45 Å for the closed and open states, respectively, and the local resolution for the TM region in the closed state was better than 2.9 Å (fig. S3), which allowed us to build precise atomic models and identify specific residues important for channel gating (figs. S4 and S5).

Conformational changes between closed and open states were large and spanned the entire molecule (fig. S6, Fig. 1A and B, and movie S1). Changes associated with Ca^{2+} binding were analyzed in three layers with different heights parallel to the membrane, i.e., the C-terminal domain (CTD), U-motif, and S4-S5 layers (Fig. 1C–E and movie S1). Upon Ca^{2+} binding, CTD rotated clockwise (Fig. 1C), U-motif rotated clockwise toward the S2-S3 domain (Fig. 1D), and S6 leaned outward from the center to open the gate accompanied by rearrangements of S1-S4 helices and outward movement of the S4-S5 linker (Fig. 1E). The C-terminal side of the central domain (C-central), U-motif, CTD, and cytoplasmic S6 ($S6_{cyto}$) were tightly attached to each other in both

closed and open states (Fig. 1F, fig. S7, and movie S2) and rotated together 9.8° clockwise with respect to the axis approximately parallel to S6 (Fig. 1G). In contrast, the N-terminal of the central domain (N-central) did not follow the rotation due to its central domain being split into two parts with G3987 as the pivot (Fig. 1F). Since the rotation axis was close to the Ca^{2+}-binding site, slight movements caused by Ca^{2+} binding resulted in very large movements around S6 (Fig. 1G).

Given these series of movements, we hypothesized the gating mechanism of RyR2 as follows: the rotation of the C-central/U-motif/$S6_{cyto}$/CTD complex upon Ca^{2+} binding leads to two downstream pathways for channel pore opening; (1) the $S6_{cyto}$ movement leads to the outward leaning of S6 and (2) the U-motif movement leads to sequential movements of the S2-S3 domain and TM segments, causing outward movement of the S4-S5 linker and creating a space where S6 can lean into. The channel pore finally opens by combining these two independent pathways (Fig. 1H). To prove this hypothesis, we performed detailed structural analysis and functional studies.

U-motif/S2-S3 domain interaction is key for signal transduction in response to Ca^{2+} binding

The U-motif/S2-S3 domain interaction is important in transducing the rotation of the U-motif in response to TM segment movement (Figs. 1D and 2A and movies S1 and S2). We found three key interactions between the U-motif and S2-S3 domain formed by hydrogen bonds or salt bridges (Fig. 2A–C, fig. S8, and movie S3). E4198-K4593-S4167 was evident in the open state, whereas Y4498-K4593 was only formed in the closed state, indicating that K4593 switches the interacting partner between both states. Additionally, E4193-R4607 was stable in both states.

To clarify the roles of hydrogen bonds/salt bridges in channel gating, functional assays were conducted with RyR2 carrying mutations at the specific residues. Ca^{2+}-dependent [^{3}H]ryanodine binding is used in functional analysis as it reflects channel activity (*12, 22*). Wild-type (WT) RyR2 exhibited biphasic Ca^{2+}-dependent [^{3}H]ryanodine binding, whereas alanine substitution at K4593 markedly this reduced binding (Fig. 2D). Two pathogenic mutations, K4593Q and K4593R (table S2), also led to loss of binding (Fig. 2E and fig. S9). Similarly, binding was not observed after alanine substitutions (Y4498A, S4167A, and E4198A) and pathogenic mutation (S4167P; table S2) in interacting partners (Fig. 2D and E and fig. S9). The phenotypes of mutant RyR2 channels were also evaluated in live cells by monitoring cytoplasmic and endoplasmic reticulum (ER) luminal Ca^{2+} homeostasis (*12, 23*). In WT RyR2-expressing HEK293 cells, spontaneous Ca^{2+} oscillations occurred with a concomitant decrease in $[Ca^{2+}]_{ER}$, indicating Ca^{2+} release from the ER via RyR2 channels (Fig. 2F, left). In contrast, RyR2 channels carrying the K4593A mutation showed no such Ca^{2+} oscillations with increased $[Ca^{2+}]_{ER}$, indicating a loss-of-function phenotype (Fig. 2F, right). Similar results were obtained with other substitutions in S4167, E4198, and K4593 (Fig. 2G). Altogether, these results suggest that both E4198-K4593-S4167 and Y4498-K4593 interactions are important for channel opening. We also evaluated the E4193-R4607 interaction and found that alanine substitutions (E4193A and R4607A) and pathogenic mutations (R4607Q and R4607W; table S2) led to a loss-of-function phenotype (Fig. 2D–G, and fig. S9). These findings indicate that three interactions above S2 in the U-motif/S2-S3 domain interface play a critical role in transducing the Ca^{2+}-binding signal to S2, and that loss of these interactions results in a loss of channel function.

Movements of the S1-S4 bundle lead to outward movement of the S4-S5 linker

Movement of the S2-S3 domain is believed to cause S2 movement (Fig. 2C). This leads to the coordinated 7.6° clockwise rotation of S1, S3, and S4 (Figs. 1E, 3A–C, and movies S1 and S4). S1, S2, S3, and S4 are arranged in a circle, placed at equal intervals in a clockwise direction (Fig.

3A–C). We found interactions between S1 and S2 (S1/S2), S2/S3, S3/S4, and S1/S4, all of which were maintained in both closed and open states (Fig. 3A and B, and movie S4). The hydrophobic interactions between F4497 and L4592 at S1/S2; hydrogen bond between Y4589 and D4715 at S2/S3; hydrogen bond between Y4720 and D4744 at S3/S4; and the salt bridge between R4501 and D4744 at S1/S4 appear to bundle the four TM segments into one (i.e., S1-S4 bundle).

Alanine substitution of residues involved in S1/S2 (F4497-L4592) and S2/S3 (Y4589-D4715) interactions exhibited significantly reduced [^{3}H]ryanodine binding (Fig. 3D and E, and fig. S10A), loss of Ca^{2+} oscillations, and increased ER Ca^{2+} (Fig. 3F and G)—all indicative of loss-of-function. The pathogenic mutant F4497C (table S2) also resulted in loss-of-function (Fig. 3E and G and fig. S10A). Thus, S1/S2 and S2/S3 interactions are necessary for channel opening. Surprisingly, alanine substitution of D4744, which is involved in both S1/S4 (R4501-D4744) and S3/S4 (Y4720-D4744) interactions, caused increased [^{3}H]ryanodine binding combined with increased Ca^{2+} sensitivity (Fig. 3D and E and fig S10A) and markedly reduced ER Ca^{2+} (Fig. 3F and G), indicating gain-of-function. Similar results were observed with alanine substitution of interacting partners (R4501 and Y4720) and two pathogenic mutants (Y4720C and D4744H; table S2) (Fig. 3E and G and fig. S10A).

Rotation of the S1-S4 bundle causes movement of the S4-S5 linker. We found that the upper part of S4 rotated 40° counterclockwise to form an α-helix upon channel opening, which dramatically changed the position of F4749 (Fig. 3H–J and movie S4). The S4-S5 linker, which is unfolded and significantly bent in the direction of S6 in the closed state, rewinds to an α-helix and moves outward (fig. S11 and movie S4). A hydrophobic interaction between F4749 in the upper part of S4 and L4505 in S1 was identified in the closed state (Fig. 3H).

Alanine substitutions of residues involved in hydrophobic interactions (L4505A and F4749A) and the pathogenic mutant L4505P (table S2) caused gain-of-function with increased Ca^{2+} sensitivity (Fig. 3K–N and fig. S10B). Notably, no additive effects were observed upon binding of [^{3}H]ryanodine to double mutant L4505A_F4749A (fig. S10B), supporting an interaction between the two residues.

Taking these findings into consideration, we hypothesized a channel opening mechanism in which a series of movements of S4-S5 linker regulate channel opening. In the absence of Ca^{2+}, the channel is stabilized in the closed state as outward movement of the S4-S5 linker is severely restricted as the "stopper," in form of L4505-F4749 interaction, prevents α-helix formation of the upper part of S4. The L4505-F4749 interaction is supported by S1/S3 and S3/S4 interactions that keep the two residues appropriately placed. Upon Ca^{2+} binding, clockwise rotation of the S1-S4 bundle induced by U-motif/S2-S3 domain interaction alters the relative positions of L4505 and F4749 to release the stopper. This allows α-helix formation of the upper part of S4 and subsequent outward movement of the S4-S5 linker to open the channel. Loss of necessary interactions, such as that of the U-motif/S2-S3 domain (Fig. 2A–C), S1/S2, and S2/S3 (Fig. 3, A–C), cannot release the stopper, leading to loss-of-function (Figs. 2D–G and 3D–G). Conversely, loss of interactions that support S4, such as S1/S4 and S3/S4 (Fig. 3A–C and H–J) destabilize of the channel in the closed state and impart a gain-of-function phenotype (Fig. 3K–N).

U-motif/$S6_{cyto}$/CTD interaction plays key role in stabilizing the channel in the closed state

The U-motif/$S6_{cyto}$/CTD complex was stable in both the closed and open states (Fig. 1F and fig. S7). We found a close contact between U-motif and $S6_{cyto}$ as observed in the closed state structure of RyR1 (*24*) (Fig. 4A and B, movie S5). In the closed state, V4176, F4173, and N4177 in the U-motif and V4879 and Q4875 in $S6_{cyto}$ faced each other forming van der Waals interactions,

and were surrounded by Q4876 and Q4878 from S6 (Fig. 4B and movie S5). In the open state, $S6_{cyto}$ self-rotated (~30º clockwise at Q4875) and U-motif/$S6_{cyto}$ loosened and appeared unstable (Fig. 4C and movie S5). Buried surface area analysis calculated by CNS (*25*) demonstrated that the U-motif/$S6_{cyto}$ interface in the open state (362 $Å^2$) was smaller than in the closed state (514 $Å^2$). The U-motif also interacted with CTD via F4888, where it penetrated partly into the hydrophobic pocket formed by U-motif F4171, I4172, and V4175 and CTD L4914 (Fig. 4D and movie S5). The U-motif/CTD interaction was stable in both states.

All alanine-substituted mutants of residues interacting between U-motif and $S6_{cyto}$ (Fig. 4E–H and fig. S12A) as well as two CPVT mutations (N4177S and N4177Y; table S2) led to gain-of-function (Fig. 4F and H and fig. S12A). Alanine substitution of F4888 exhibited severe gain-of-function with increased Ca^{2+} sensitivity (Fig. 4I–L and fig. S12B). Similar results were obtained with F4888Y (table S2), a pathogenic mutant (Fig. 4J and L, and fig. S12B). Alanine substitution of F4171, I4172, V4175, and L4914—involved in the hydrophobic pocket—also led to gain-of-function (Fig. 4I–L, and fig. S12B). The double mutant N4177A_F4888A showed similar to single mutants, indicating common pathways for both after loss of U-motif/$S6_{cyto}$ and U-motif/CTD interactions (fig. S12B). These findings suggest that interactions within the U-motif/$S6_{cyto}$/CTD complex play a key role in stabilizing the closed channel.

Structural basis of the gain-of-function mutations

To elucidate the structural changes associated with underlying gain-of-function mutants, we conducted structural analysis of two mutants (F4749A and F4888A). Two different classes (closed/open-like structures) were obtained for both mutants in the presence of EGTA (figs. S13 and S14) and Ca^{2+} was bound in the open-like structures. This was not observed for the WT structure in the presence of EGTA, reflecting the result of increasing Ca^{2+} sensitivity in both mutants (Figs. 3K and 4I). We also determined the structure in the presence of 100 μM Ca^{2+} for F4749A, and found essentially the same structure as that of open-like F4749A in the presence of EGTA. The overall resolution of the final models was 3.2–3.8 Å (figs. S15 and S16, and table S1), which was sufficient to analyze structural changes induced by mutations (figs. S17 and S18).

Unexpectedly, there was no notable difference between WT and F4749A in TM segments and S4-S5 linker as well as overall structure in the closed state (Fig. 5A and fig. S20A). This indicates that breaking the stopper does not induce spontaneous conformation changes in the S4-S5 linker or TM segments. In contrast, appreciable change was detected in the U-motif in the closed F4888A structure (Fig. 5B and C, figs. S19 and S21A, and movie S6), although no differences were observed in the TM segments (fig. S21B). Replacing the phenyl group with a methyl group created an extra space above F4171, causing the α-helix in the N-terminal U-motif to rotate ~15° clockwise around F4171 with respect to the WT in the closed state (Fig. 5B and C, fig. S19, and movie S6). Consequently, F4171 moved up to fill the space and the interaction between U-motif and $S6_{cyto}$ became loose, as if the mutant partially mimicked the U-motif conformational change of the open state WT (Fig. 5B and C, and movie S6).

In the open state, F4888A differed from WT; first, there was a parallel movement of the U-motif, S2-S3 domain, and S1-S4 toward the outside (Fig. 5D and E), which differed from the rotational motion observed in the WT structural change from closed to open states. The S4-S5 linker, S5, and S6 showed only a slight outward movement (Fig. 5E and fig. S21, C and D). Movement of the U-motif in the mutant created a different environment from that of the open state WT U-motif/$S6_{cyto}$ interaction (Fig. 5F). Moreover, the buried surface area of the U-motif/$S6_{cyto}$ interface (335 $Å^2$) was smaller than that of the open state WT (362 $Å^2$). As a result, mutants could

not easily return to the closed state and might have longer channel pore openings than the WT, resulting in gain-of-function. Movements observed in the open F4888A were also detected in the open F4749A (fig. S20); subtle movements of the S4-S5 linker and S6 (fig. S20, C and D) might have altered the U-motif/$S6_{cyto}$ interaction (Fig. 5D–F, and fig. S21, C to D). Thus, similar structural changes were observed for the two mutants with different points of action and this gain-of-function occurred via a common mechanism.

Discussion

By combining high-resolution cryo-EM structures and quantitative functional analysis of mutants generated based on these structures, we successfully clarified the gating mechanism of RyR2 upon Ca^{2+} binding. Conformation changes associated with Ca^{2+} binding are regulated by a number of rotations of domains/α-helix and domain-domain interactions. Accordingly, we propose the following channel opening mechanism: (1) rotation of the U-motif unit causes S6 movement; (2) U-motif/S2-S3 domain interaction transduces the signal to S2; (3) rotation of the S1-S4 bundle releases the stopper comprising F4749/L4505; (4) rotation of the upper part of S4 induces outward movement of the S4-S5 linker, creating a space where S6 can lean into; and (5) rotation of $S6_{cyto}$ loosens the U-motif/$S6_{cyto}$ interaction, initiating the outward leaning of S6 (Fig. 6).

Mutations of residues involved in the signaling pathway induced outward movement of the S4-S5 linker, causing loss-of-function, whereas those supporting the stopper (i.e., S1/S3/S4 and S1/S4 interactions) or the U-motif/CTD/$S6_{cyto}$ complex led to gain-of-function. We identified six loss-of-function (S4167P, F4497C, K4593Q, K4593R, R4607Q, and R4607W) and seven gain-of-function (N4177S, N4177Y, L4505P, Y4720C, D4744H, V4879A, and F4888Y) pathogenic mutations in the expected locations. Given the locations of these mutations (Fig. 6A), it becomes apparent that mutation of the amino acid residues involved in interactions at and near the S6 segment (i.e. inner region) of the molecule lead to gain-of function, whereas mutation of those involved in interactions in the outer region lead to loss-of-function. This highlights that interactions in the core region are essential for stabilizing the channel in the closed state and those in the surrounding region are essential for regulating channel opening.

Outward movement of the S4-S5 linker in the open state is important, as it creates the space where S6 can lean into (*15, 26*). des Georges et al. (*26*) provide a more detailed description where the S4-S5 linker, which is bent in the direction of S6 in the closed state and holds it in place, straightens and alters its contacts with S6, thereby opening the channel pore. These findings are in line with our results. We further demonstrated that rewinding of the upper S4 part to an α-helix, caused by rotation of the S1-S4 bundle, drives the significant S4-S5 linker movement.

In RyR1, rearrangement of the salt bridges between S1 (R4563), S3 (Y4791) and S4 (D4815) has been reported to occur upon channel opening (*26*). We showed that the corresponding salt bridges between R4501, Y4720, and D4744 were preserved in RyR2 but maintained in both closed and open states. Functional assays revealed that hydrogen bonds/salt bridges are critical to keep the stopper in place, as disruption of salt bridges by alanine substitutions or pathogenic mutations caused severe gain-of-function of the channel. Interestingly, a recent study showed that diamide insecticides bind to the pocket within the S1-S4 bundle of RyR1, thereby disrupting the salt bridge and opening RyR1(*27*). Our results explain why such insecticides activate the RyR channel.

The U-motif is believed to be important in channel gating as it forms a stable complex with $S6_{cyto}$ and CTD, which move together when the channel opens (*24*). This movement is accompanied by a rigid shift in the S2-S3 domain, which has been proposed to eventually open the channel pore (*28*); these findings are in agreement with our results. We further found that the

U-motif/CTD/$S6_{cyto}$ complex and C-central form a super-complex and that rotates upon Ca^{2+} binding. We also demonstrated that the interaction between U-motif and the S2-S3 domain transmits signal between Ca^{2+} binding and TM rearrangements; indeed, loss of the U-motif/S2-S3 domain interaction prevented channel opening. The U-motif/$S6_{cyto}$ interaction has also been highlighted in channel opening (*24*), and we have successfully confirmed its importance in stabilizing the channel in the closed state; we demonstrated that the U-motif/$S6_{cyto}$ interface in the open state was smaller than that in the closed state and that mutations inhibiting U-motif/$S6_{cyto}$ interaction caused gain-of-function of the channel. We further highlighted the importance of the U-motif/CTD interaction, as mutations in F4888 caused gain-of-function and reduced stability of the U-motif/$S6_{cyto}$/CTD complex as confirmed by the structure of closed-like F4888A. These findings suggest that the U-motif is bifunctional: it plays an important role in both opening the channel and stabilizing the channel in the closed state. Indeed, local conformation changes within the U-motif occurred in the F4888A mutant structure, which subsequently loosened the U-motif/$S6_{cyto}$ interaction. As a result, the rotation of the CTD/U-motif upon Ca^{2+}-binding may be more likely to occur.

In RyRs, the large cytoplasmic region is believed to play an important role in regulating channel opening. Indeed, a number of pathogenic mutations is located in the cytoplasmic region. Large downward movement of the cytoplasmic region accompanied by considerable changes in inter-domain interactions was demonstrated during RyR2 channel opening (*15*). The overall motion of the region may result from domain-wise displacement and relative shifts between domains through conformational changes in the central domain upon Ca^{2+} binding (*15, 28*). Recently, RyR1 and RyR2 structures carrying gain-of-function mutations at N-terminal domains (NTD) were reported (*29*). Determining the structures of various mutant RyRs will help to elucidate the long-range allosteric gating mechanism in the future.

Gain-of-function and loss-of-function mutations cause different diseases; the former are responsible for CPVT and LVNC (*5, 8-10*) and the latter IVF and LQTS (*12-14, 30*). Different drugs are required to treat these diseases, such as RyR2 inhibitors for gain-of-function mutations and RyR2 activators for loss-of-function mutations. Thus, our findings may be useful for drug design, as compounds that efficiently weaken or strengthen specific interactions can be powerful drug candidates. For example, compounds that weaken interactions in the outer region (e.g., U-motif/S2-S3) can be used for treating gain-of-function diseases.

In conclusion, we have revealed the gating mechanism of RyR2 upon Ca^{2+} binding through newly determined structures and functional assays, and provided structural insights into the effects of pathogenic mutations on channel activity that may help develop more effective drugs to treat RyR2-associated diseases.

References and notes

1. M. Endo, Calcium-induced calcium release in skeletal muscle. *Physiol Rev* **89**, 1153-1176 (2009).
2. A. Fabiato, F. Fabiato, Calcium-induced release of calcium from the sarcoplasmic reticulum of skinned cells from adult human, dog, cat, rabbit, rat, and frog hearts and from fetal and new-born rat ventricles. *Ann NY Acad Sci* **307**, 491-522 (1978).
3. O. B. Clarke, W. A. Hendrickson, Structures of the colossal RyR1 calcium release channel. *Curr Opin Struct Biol* **39**, 144-152 (2016).
4. R. Zalk, A. R. Marks, Ca^{2+} release channels join the "resolution revolution". *Trends Biochem Sci* **42**, 543-555 (2017).
5. S. G. Priori *et al.*, Clinical and molecular characterization of patients with catecholaminergic polymorphic ventricular tachycardia. *Circulation* **106**, 69-74 (2002).
6. D. J. Tester, D. B. Spoon, H. H. Valdivia, J. C. Makielski, M. J. Ackerman, Targeted mutational analysis of the RyR2-encoded cardiac ryanodine receptor in sudden unexplained death: a molecular autopsy of 49 medical examiner/coroner's cases. *Mayo Clin Proc* **79**, 1380-1384 (2004).
7. M. Kawamura *et al.*, Genetic background of catecholaminergic polymorphic ventricular tachycardia in Japan. *Circ J* **77**, 1705-1713 (2013).
8. A. R. Pérez-Riera *et al.*, Catecholaminergic polymorphic ventricular tachycardia, an update. *Ann Noninvas Electrocardiol* **23**, e12512 (2018).
9. S. Ohno *et al.*, Exon 3 deletion of RYR2 encoding cardiac ryanodine receptor is associated with left ventricular non-compaction. *Europace* **16**, 1646-1654 (2014).
10. Y. Nozaki *et al.*, Co-phenotype of left ventricular non-compaction cardiomyopathy and atypical catecholaminergic polymorphic ventricular tachycardia in association with R169Q, a ryanodine receptor type 2 missense mutation. *Circ J* **84**, 226-234 (2020).
11. Y. Tang, X. Tian, R. Wang, M. Fill, S. R. Chen, Abnormal termination of Ca^{2+} release is a common defect of RyR2 mutations associated with cardiomyopathies. *Circ Res* **110**, 968-977 (2012).
12. Y. Fujii *et al.*, A type 2 ryanodine receptor variant associated with reduced Ca^{2+} release and short-coupled torsades de pointes ventricular arrhythmia. *Heart Rhythm* **14**, 98-107 (2017).
13. D. Jiang, W. Chen, R. Wang, L. Zhang, S. R. Chen, Loss of luminal Ca^{2+} activation in the cardiac ryanodine receptor is associated with ventricular fibrillation and sudden death. *Proc Natl Acad Sci U S A* **104**, 18309-18314 (2007).
14. C. Paech *et al.*, Ryanodine receptor mutations presenting as idiopathic ventricular fibrillation: a report on two novel familial compound mutations, c.6224T>C and c.13781A>G, with the clinical presentation of idiopathic ventricular fibrillation. *Pediatr Cardiol* **35**, 1437-1441 (2014).
15. W. Peng *et al.*, Structural basis for the gating mechanism of the type 2 ryanodine receptor RyR2. *Science* **354**, (2016).
16. D. S. Gong *et al.*, Modulation of cardiac ryanodine receptor 2 by calmodulin. *Nature* **572**, 347-351 (2019).
17. X. Chi *et al.*, Molecular basis for allosteric regulation of the type 2 ryanodine receptor channel gating by key modulators. *Proc Natl Acad Sci U S A* **116**, 25575-25582 (2019).

18. H. Ogawa, N. Kurebayashi, T. Yamazawa, T. Murayama, Regulatory mechanisms of ryanodine receptor/Ca^{2+} release channel revealed by recent advancements in structural studies. *J Muscle Res Cell Motil*, (2020).
19. V. Cabra, T. Murayama, M. Samsó, Ultrastructural analysis of self-associated RyR2s. *Biophys J* **110**, 2651-2662 (2016).
20. G. Meissner, Ryanodine receptor/Ca^{2+} release channels and their regulation by endogenous effectors. *Annu Rev Physiol* **56**, 485-508 (1994).
21. Y. Ogawa, Role of ryanodine receptors. *Crit Rev Biochem Mol Biol* **29**, 229-274 (1994).
22. T. Murayama *et al.*, A tryptophan residue in the caffeine-binding site of the ryanodine receptor regulates Ca^{2+} sensitivity. *Commun Biol* **1**, 98 (2018).
23. A. Uehara *et al.*, Extensive Ca^{2+} leak through K4750Q cardiac ryanodine receptors caused by cytosolic and luminal Ca^{2+} hypersensitivity. *J Gen Physiol* **149**, 199-218 (2017).
24. Z. Yan *et al.*, Structure of the rabbit ryanodine receptor RyR1 at near-atomic resolution. *Nature* **517**, 50-55 (2015).
25. A. T. Brünger *et al.*, Crystallography & NMR system: A new software suite for macromolecular structure determination. *Acta Crystallogr D* **54**, 905-921 (1998).
26. A. des Georges *et al.*, Structural basis for gating and activation of RyR1. *Cell* **167**, 145-157.e17 (2016).
27. R. Ma *et al.*, Structural basis for diamide modulation of ryanodine receptor. *Nat Chem Biol* **16**, 1246-1254 (2020).
28. X. C. Bai, Z. Yan, J. P. Wu, Z. Q. Li, N. Yan, The Central domain of RyR1 is the transducer for long-range allosteric gating of channel opening. *Cell Res* **26**, 995-1006 (2016).
29. K. A. Iyer *et al.*, Structural mechanism of two gain-of-function cardiac and skeletal RyR mutations at an equivalent site by cryo-EM. *Sci Adv* **6**, eabb2964 (2020).
30. D. Shigemizu *et al.*, Exome analyses of long QT syndrome reveal candidate pathogenic mutations in calmodulin-interacting genes. *PLOS ONE* **10**, e0130329 (2015).

Acknowledgments: We thank Mariko Kurakata for assistance with cell culture. We thank Ikue Hiraga and the Laboratory of Radioisotope Research, Research Support Center, Juntendo University Graduate School of Medicine, for technical assistance. We also thank the staff scientists at the University of Tokyo's cryo-EM facility. **Funding:** This study was partly supported by the Japan Society for the Promotion of Sciences KAKENHI (grant number JP16H04748 to H.O., 19K07105 to N.K., and 19H03404 to T.M.); the Platform Project for Supporting Drug Discovery and Life Science Research (Basis for Supporting Innovative Drug Discovery and Life Science Research [BINDS]; grant number JP20am0101080 to H.O. and T.M.); the Practical Research Project for Rare/Intractable Diseases from the Japan Agency for Medical Research and Development (AMED; grant number 19ek0109202) to N.K.); an Intramural Research Grant (29-4 and 2-5) for Neurological and Psychiatric Disorders of NCNP (to T.M.); and the Vehicle Racing Commemorative Foundation (to H.O. and T.M.). **Author contributions:** T.K., N.K., T.M., and H.O. conceived and designed the project. M.Ko. and H.O. performed cell culture. T.K. performed protein purification. K.S. performed negative-staining EM studies. A.T. and T.K. prepared the grid for cryo-EM. A.T. and M.Ki. processed the images. H.O. performed model building and refinement. T.M. and N.K. performed the functional analysis. T.K., A.T., N.K., K.S., M.Ko., T.S. M.Ki., T.M., and H.O interpreted the data. T.M. and H.O supervised the project. H.O. and T.M. wrote the manuscript with input from all authors. **Competing interests:** The authors declare no competing interests. **Data and materials availability:** Atomic coordinates and cryo-EM density

maps have been deposited in the PDB and the Electron Microscopy Data Bank under the accession codes 7FJ6 and EMD-30688 (closed state before classification), 7FJ7 and EMD-30689 (closed state class1), 7FJ8 and EMD-30690 (closed state class2), 7FJ9 and EMD-30691 (open state class1), 7FJA and EMD-30692 (open state class2), 7FJB and EMD-30693 (open state class3), 7FJD and EMD-30694 (closed-like F4749A mutant in the presence of EGTA), 7FJE and EMD-30695 (open-like F4749A mutant in the presence of EGTA), 7FJF and EMD-30696 (F4749A mutant in the presence of 100 μM of Ca^{2+}), 7FJG and EMD-30697 (closed-like F4888A in the presence of EGTA), and 7FJH and EMD-30698 (open-like F4888A in the presence of EGTA).

Supplementary Materials:

Materials and Methods

Figures S1-S21

Tables S1-S2

Movies S1-S6

References (1-30)

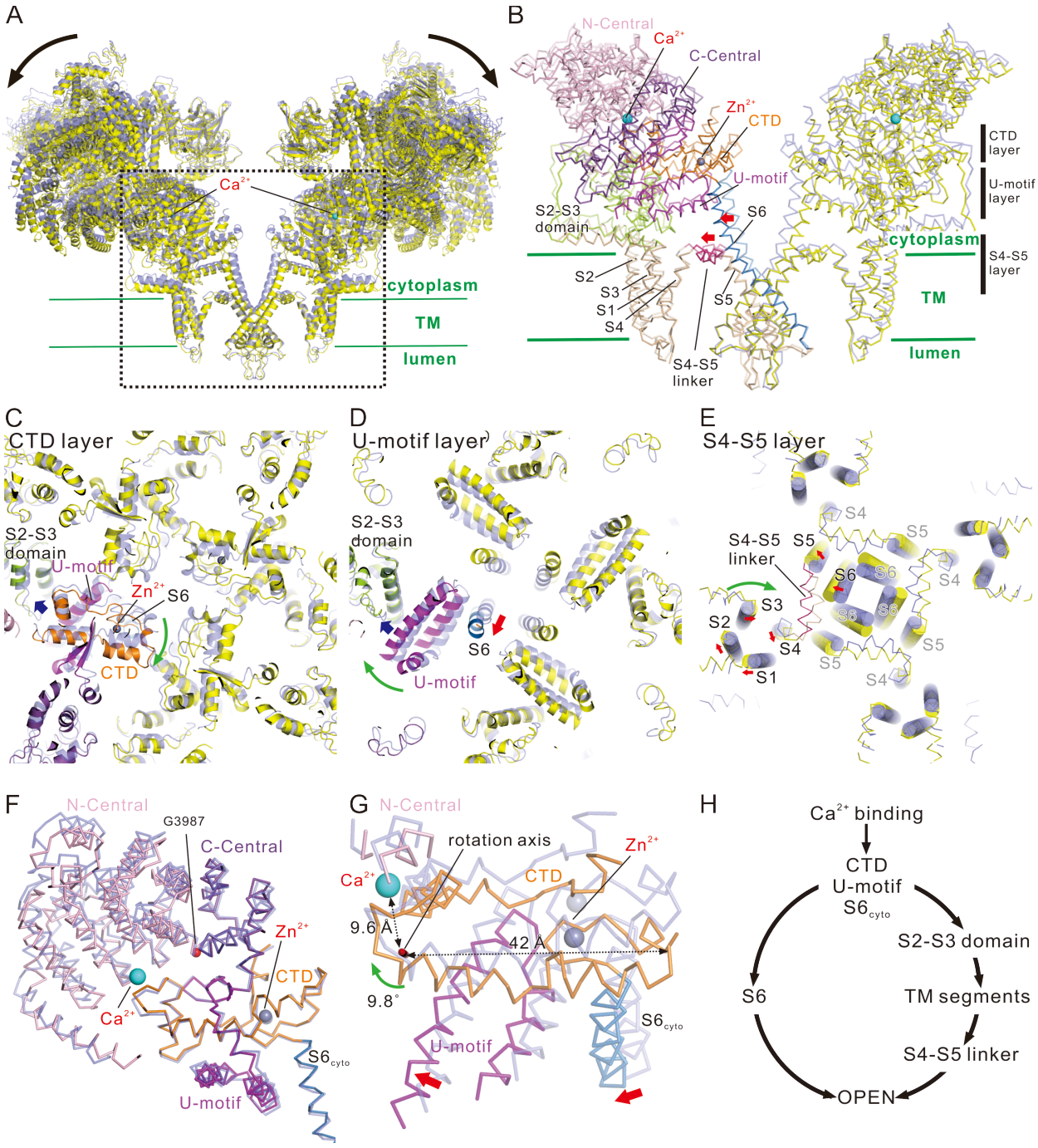

Fig. 1. Conformational changes upon Ca^{2+} binding. (A) Overlay of RyR2 in the closed (light blue) and open (yellow) states viewed from the direction parallel to the lipid bilayer and shown as a ribbon model. Two facing protomers in the RyR2 tetramer are shown. (B) Magnified view of the dotted box in (A). In the left protomer, each domain is colored (N-central, light pink; C-central, purple; U-motif, magenta; S1-S5, wheat; S2-S3 domain, light green; S4-S5 linker, warm pink; S6, blue; CTD, orange). S4-S5 linker and S6 moved outside upon Ca^{2+} binding as indicated by the red arrows. Three regions parallel to the membrane are defined as CTD, U-motif, and S4-S5 layers. Ca^{2+}, shown as cyan ball; Zn^{2+}, shown as gray ball. (C–E) Cross-section views of CTD, U-motif,

and S4-S5 layers. Closed state is colored in light blue and open state is colored according to (B) or yellow. In (E), Cα representation overlaid with cylindrical TM helices are used. Ca^{2+} binding causes clockwise rotation of CTD (green arrow in C), U-motif (green arrow in D), and S1-S4 TM helices and outward movement of S4-S5 linker and S6 (red arrows in E). (F) C-central/U-motif/$S6_{cyto}$/CTD complex. Closed (light blue) and open (colored according to B) states are overlaid at the CTD. Central domain is split into two parts with G3987 as the pivot upon Ca^{2+} binding. (G) Rotation of the C-central/U-motif/$S6_{cyto}$/CTD complex upon Ca^{2+} binding viewed from the rotation axis. (G) Movement of S2-S3 domain accompanied by rotation of the U-motif. (H) Two independent hypothetical pathways for pore opening upon Ca^{2+} binding.

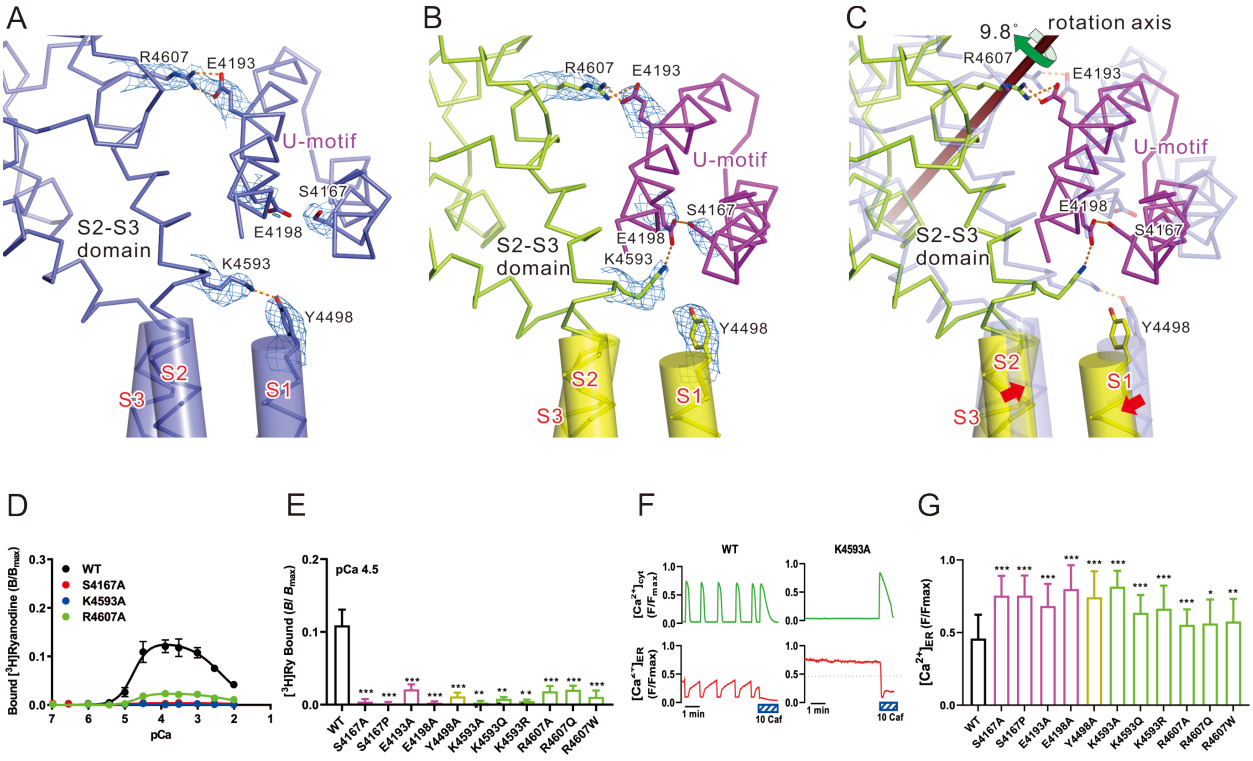

Fig. 2. Key interactions between U-motif and S2-S3 domain upon channel opening. (A–C) Interface of U-motif and S2-S3 domain in the closed state (A), open state (B), and an overlay of both states (C) viewed parallel to the membrane and shown as a Cα model. Amino acid residues involved in key interactions are shown as stick models. The color of carbon atoms is the same as that of Cα; oxygen, red; nitrogen, blue. The TM region is indicated in yellow and the region forming α-helices is overlaid with the cylinder model. Hydrogen bonds or salt bridges are shown as orange dotted lines. Density maps around side chains shown in (A) and (B) are superimposed and contoured at 0.025. (D–G) Functional analysis of mutants involved in U-motif/S2-S3 domain interaction. (D) Ca^{2+}-dependent [^{3}H]ryanodine binding of WT and representative mutants. (E) Summary of [^{3}H]ryanodine binding of WT and mutants at pCa 4.5. (F) Representative traces of cytoplasmic ($[Ca^{2+}]_{cyt}$) and ER ($[Ca^{2+}]_{ER}$) Ca^{2+} signals of HEK293 cells expressing WT or K4593A. Spontaneous Ca^{2+} oscillations occurred with a concomitant decrease in $[Ca^{2+}]_{ER}$ in WT, while the K4593 mutant showed no Ca^{2+} oscillations with an increased $[Ca^{2+}]_{ER}$, indicating loss-of-function phenotype. (G) Upper level of $[Ca^{2+}]_{ER}$ signals in the various mutants. All mutants showed loss-of-function phenotypes. Data are presented as the mean ± SD. *$p < 0.05$; **$p < 0.01$; ***$p < 0.0001$.

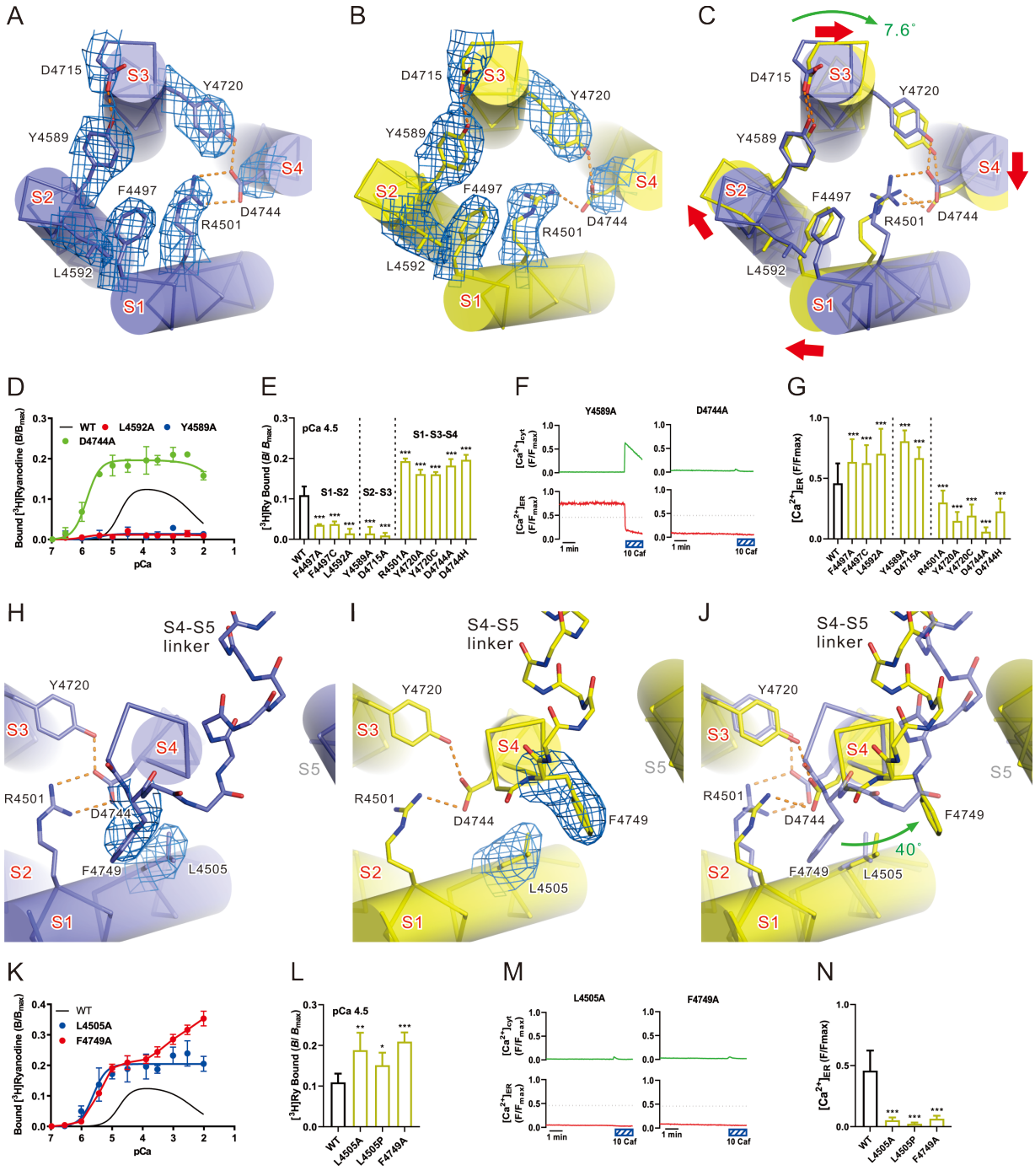

Fig. 3. Key interactions in the transmembrane region upon channel opening. (A–C) The S1-S4 bundle. Closed state (A), open state (B), and overlay of the structures in both states (C) are shown as a Cα model and overlaid with cylinder models. Hydrogen bonds/salt bridges are shown as orange botted lines. Density maps around side chains shown in (A) and (B) are superimposed and contoured at 0.03. (D–G) Functional analysis of mutants involved in the S1/S2 or S2/S3 interaction. (D) Ca^{2+}-dependent [^{3}H]ryanodine binding of WT and representative mutants. (E) [^{3}H]Ryanodine binding of WT and all mutants at pCa 4.5. (F) Representative traces of $[Ca^{2+}]_{cyt}$ and $[Ca^{2+}]_{ER}$ signals of HEK293 cells expressing Y4589A or D4744A. (G) Upper level of $[Ca^{2+}]_{ER}$

signals in all mutants. (H–J) TM region around S4. Closed state (H), open state (I), and overlay of the structures in both states (J). Structures in both states were fitted to the bottom part of S4 helices and viewed along the axis of the S4 helix and from the cytoplasm; Cα model overlaid with cylinder models. Main chain representation of the S4-S5 linker. Density maps around side chains shown in (H) and (I) are superimposed and contoured at 0.03. (K) Ca^{2+}-dependent [^{3}H]ryanodine binding of WT and representative mutants. (L) [^{3}H]Ryanodine binding of WT and all mutants at pCa 4.5. (M) Representative traces of $[Ca^{2+}]_{cyt}$ and $[Ca^{2+}]_{ER}$ signals of HEK293 cells expressing L4505A or F4749A. (N) Upper level of $[Ca^{2+}]_{ER}$ signals in all mutants.

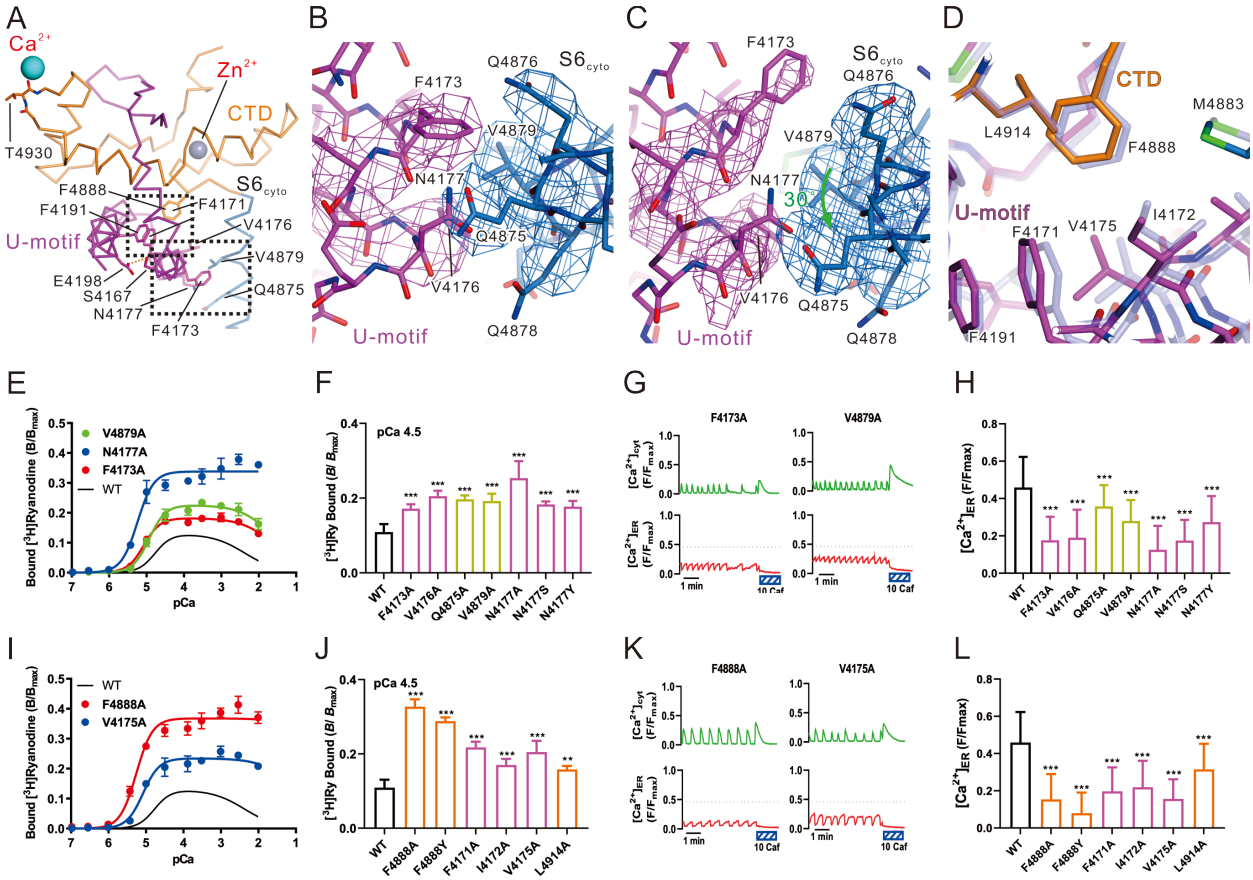

Fig. 4. Key interactions between the U-motif and S6$_{cyto}$/CTD. (A) Structure around the U-motif in the open state (U-motif, magenta; S6$_{cyto}$, blue; CTD, orange). Ca^{2+} and Zn^{2+} are shown as cyan and gray spheres, respectively. (B, C) Details of the U-motif/S6$_{cyto}$ interaction. Structures in the closed (B) and open (C) states fitted to the N-terminal region of the U-motif are shown as a full atomic model. Density maps around the interaction are superimposed and contoured at 0.025. (D) Details of the U-motif/CTD interaction around F4888. Overly of the structures in the closed (light blue) and open (colored) states. (E–L) Functional analysis of mutants involved in U-motif/S6$_{cyto}$ (E–H) and U-motif/CTD (I–L) interactions. (E, I) Ca^{2+}-dependent [^{3}H]ryanodine binding of WT and representative mutants, and (F, J) all mutants at pCa 4.5. (G, K) Representative traces of $[Ca^{2+}]_{cyt}$ and $[Ca^{2+}]_{ER}$ signals of HEK293 cells expressing F4173A or V4879A (G) and F4888A or V4175A (K). (H, L) Upper level of $[Ca^{2+}]_{ER}$ signals in all mutants.

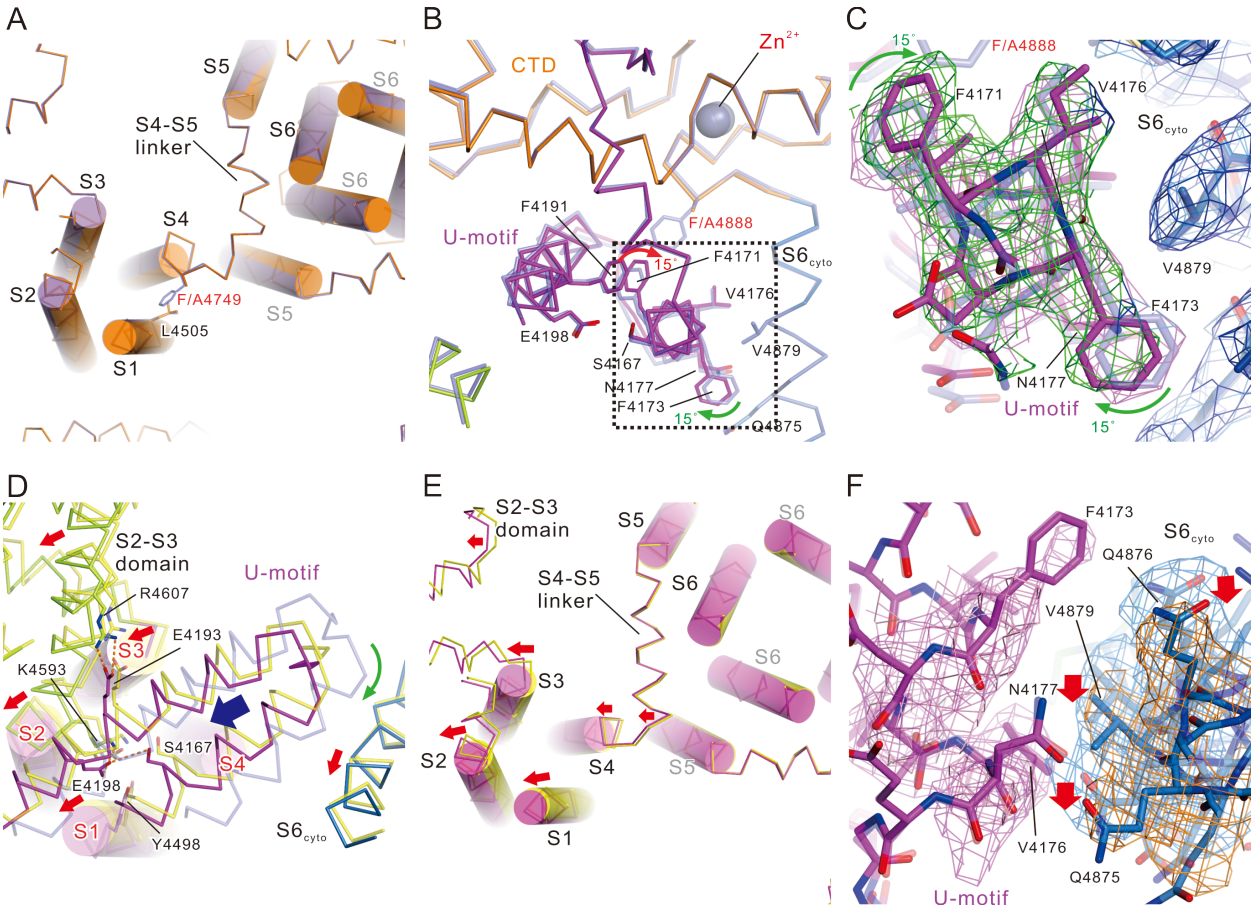

Fig. 5. Structural basis of gain-of-function mutations. (A) Overlay of closed-like F4749A (orange) and WT in the closed state (light blue) at the TM region viewed from the cytoplasm. (B) Structure of closed-like F4888A (colored) overlaid with WT in the closed state (light blue). (C) Enlarged view of the dotted box in (B) superposed with density maps contoured at 0.025. Magenta and green nets represent density maps around WT U-motif in the closed state and closed-like F4888A, respectively. Light blue and blue nets represent density maps around WT $S6_{cyto}$ in the closed state and closed-like F4888A, respectively. (D) Interface of U-motif and S2-S3 domain of open-like F4888A (colored) overlaid with WT in the open state (yellow) and in the closed state (only U-motif is shown, blue). Note that in the mutant, parallel movement of the U-motif and S2-S3 domains toward the outside compared with the WT in the open state is completely different from the rotation motion seen in the WT structural change from closed to open state. (E) Overlay of the TM region of open-like F4888A (violet) with WT in the open state (yellow). (F) Details of the U-motif/$S6_{cyto}$ interaction. Open-like F4888A and WT in the open states fitted to the N-terminal region of the U-motif are superposed with density maps contoured at 0.025. Magenta and light pink nets represent density maps around the WT U-motif in the open state and open-like F4888A, respectively. Light blue and orange nets represent density maps around WT $S6_{cyto}$ in the open state and open-like F4888A, respectively.

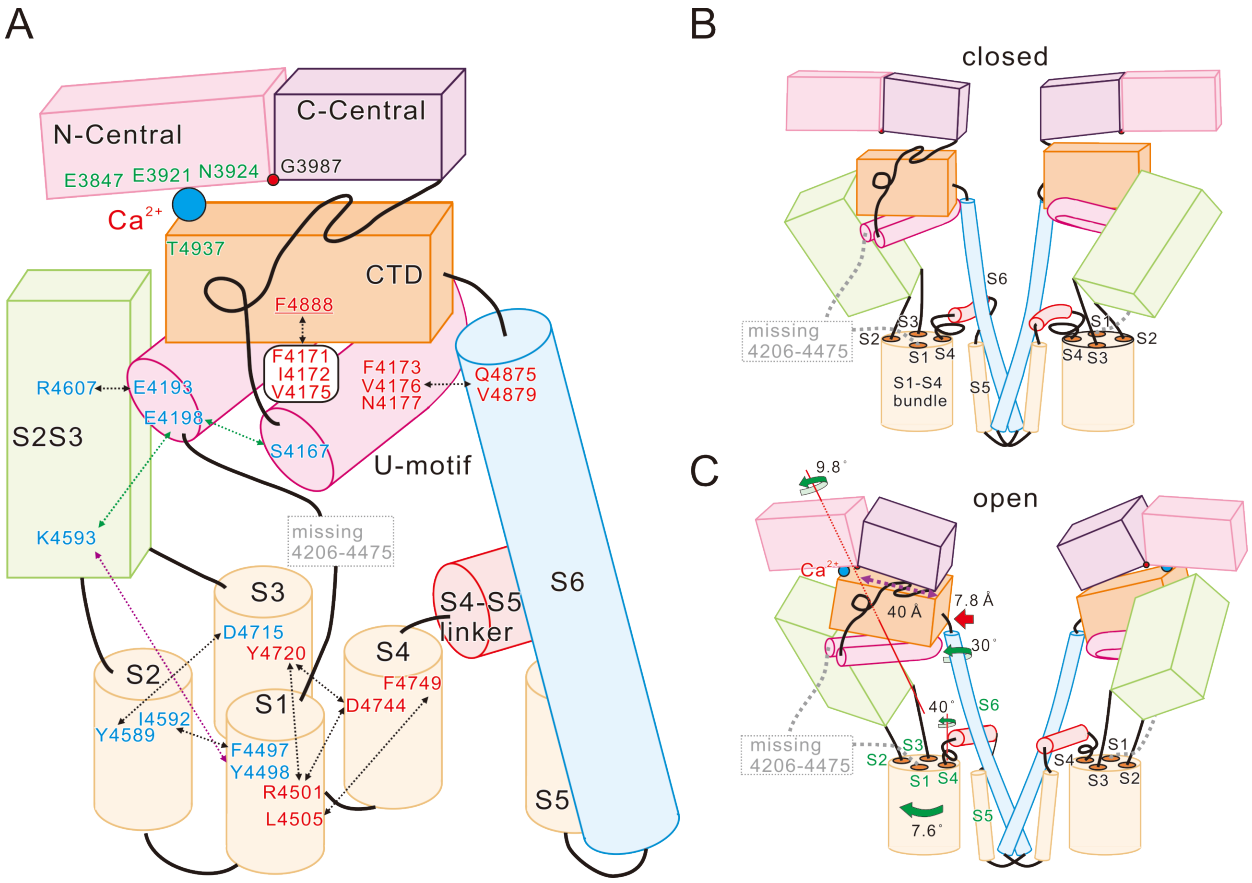

Fig. 6. Schematic diagram of the RyR2 channel gating mechanism upon Ca^{2+} binding. (A) Details of interactions identified in this study. Amino-acid residues shown in red letter and blue letter indicate gain-of-function and loss-of-function by these mutations, respectively. Arrows indicate interactions. Yellow and dark blue arrows indicate interactions only found in the closed and open states, respectively. (B, C) Scheme of the structure in the closed (B) and open (C) state. In the closed state, the upper part of S4 does not form an α-helix. The S4-S5 linker is unfolded and significantly bends in the direction of S6. Binding of Ca^{2+} to the C-central/CTD interface causes 9.8° rotation of the C-central/U-motif/$S6_{cyto}$/CTD complex, leading to two pathways. Pathway 1: the rotation causes 30º rotation of $S6_{cyto}$ which loosens the U-motif/$S6_{cyto}$ interaction and allows outward movement of S6. Pathway 2: a sequential movement of the S2S3 domain, S2, S1-S4 bundle, and S4 allows the upper part of S4 to rewind and form an α-helix. Subsequently, the S4-S5 linker moves outward, creating a space where S6 can lean into. A combination of these two independent pathways eventually leads to opening of the channel.